Hindawi
Mathematical Problems in Engineering
Volume 2018, Article ID 6134764, 10 pages
https://doi.org/10.1155/2018/6134764

Research Article

Trajectory Design and Tracking Control for Nonlinear Underactuated Wheeled Inverted Pendulum

Shuli Gong[1], **Ancai Zhang**[2,3,4], **Jinhua She**[3,5], **Xinghui Zhang**[2,4] and **Yuanyuan Liu**[1]

[1] *School of Mathematics and Statistics, Linyi University, Linyi, Shandong 276005, China*
[2] *School of Automation and Electrical Engineering, Linyi University, Linyi, Shandong 276005, China*
[3] *School of Engineering, Tokyo University of Technology, Hachioji, Tokyo 192-0982, Japan*
[4] *Key Laboratory of Complex Systems and Intelligent Computing in Universities of Shandong, Linyi, Shandong 276000, China*
[5] *School of Automation, China University of Geosciences, Wuhan, Hubei 430074, China*

Correspondence should be addressed to Ancai Zhang; zhangancai123@hotmail.com

Received 4 July 2018; Accepted 3 September 2018; Published 24 September 2018

Academic Editor: Ju H. Park

An underactuated wheeled inverted pendulum (UWIP) is a nonlinear mechanical system that has two degrees of freedom and has only one control input. The motion planning problem for this nonlinear system is difficult to solve because of the existence of an uncontrollable manifold in the configuration space. In this paper, we present a method of designing motion trajectory for this underactuated system. The design of trajectory is based on the dynamic properties of the UWIP system. Furthermore, the tracking control of the UWIP for the constructed trajectory is also studied. A tracking control law is designed by using quadratic optimal control theory. Numerical simulation results verify the effectiveness of the presented theoretical results.

1. Introduction

There are many complex dynamic systems in nature. The nonlinear system is an important type of natural system. Since this kind of system can more accurately reflect the essential characteristics of natural systems, they have been attracting more and more attention in the past few decades. Researchers have carried out intensively study on the dynamic analysis and control problem for the nonlinear systems [1–8].

Recently, the control of the nonlinear underactuated mechanical system (UMS) is a hot issue in the engineering area. A UMS has fewer actuators than degrees of freedom (DOF) [9]. There are many examples of the UMS in our daily life. Those include a surface vessel [10], a VTOL aircraft [11], a bridge crane [12], an underwater vehicle [13], and a helicopter [14]. The reduction of actuators makes the UMS have light weight, low energy consumption, flexible movement, and other features. It has wide application prospects in many fields.

However, the control problems presented by the UMS are not easy to solve because of the following two reasons. First, the UMS usually has complex nonlinear dynamics and does not be strict feedback linearized [15]. Second, the UMS has nonholonomic constraints due to the reduction of actuators [16]. This means that the state variables of UMS are located in an uncontrollable manifold in the configuration space. The control of the UMS is a challenging problem in the nonlinear control area.

In order to conveniently study the control theory of the UMS, some experimental models of the UMS have been built in a lab environment (e.g., Acrobot [17], Furuta pendulum [18], Beam-ball [19], and TORA [20]). Based on these models, many nonlinear control methods have been developed, for example, an equivalent input disturbance (EID) method in [21], an energy-based and nonsmooth Lyapunov function method in [22], a reduced-order control method in [23], and a PID passivity-based method in [24].

An underactuated wheeled inverted pendulum (UWIP) is a recent presented lab model of the UMS [25]. This mechanical system has a wheel and an inverted pendulum (see Figure 1). An actuator drives the wheel to move in a horizontal plane. And the inverted pendulum can freely rotate in a vertical plane. The UWIP is a 2-DOF complex nonlinear system that is not strict feedback linearizable. It

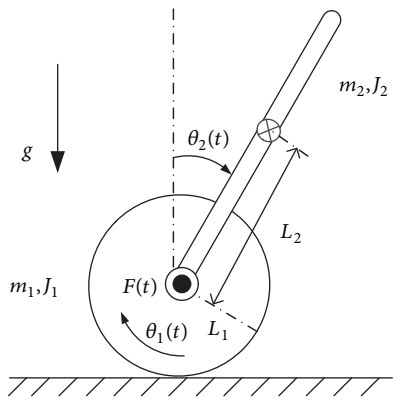

Figure 1: Underactuated wheeled inverted pendulum (UWIP).

has a second-order nonholonomic constraint and has an uncontrollable passive DOF. All these make the motion control of the UWIP system be difficult to solve. So far, there are no research results about the motion planning of the system. This inspires the study in this paper. We solve this difficult problem in this study. First, the dynamic properties of the UWIP system are analyzed. Based on these properties, a method of constructing a motion trajectory for this mechanical system is developed. The trajectory starts from the straight-down equilibrium point and ends at the straight-up equilibrium point. After that, a tracking control law is designed to quickly track the constructed trajectory. This enables the stabilizing control of the UWIP between two equilibrium points to be achieved along a reference trajectory. Compared to a local stabilizing control method for the UWIP in [25], our presented strategy uses a single control law to achieve the stabilizing control of the UWIP in its whole motion space. Moreover, we can predict the movement process and transient characteristics of the UWIP in advance. It is very useful to guarantee the operation of the control system to be safe. The validity of the theoretical results is demonstrated by numerical simulation experiment.

2. Model of Underactuated Wheeled Inverted Pendulum

The model of the UWIP is shown in Figure 1, where m_1, J_1, L_1, and $\theta_1(t)$ are the mass, the moment of inertia, the radius, and the rotational angle of the wheel, respectively; m_2, J_2, L_2, and $\theta_2(t)$ are the mass, the moment of inertia, the distance from the endpoint to the center of mass, and the rotational angle of the pendulum, respectively; $F(t)$ is the input torque applied on the wheel; $g = 9.80665\, m/s^2$ is the gravitational acceleration.

It follows from the derivations in [25] that the kinetic and potential energy of the UWIP system is

$$\begin{aligned} K\left(\boldsymbol{\theta}, \dot{\boldsymbol{\theta}}\right) &= \frac{1}{2}\dot{\boldsymbol{\theta}}(t)^{\top} D\left(\theta_2\right)\dot{\boldsymbol{\theta}}(t), \\ P(\boldsymbol{\theta}) &= \alpha_4 \cos\theta_2(t), \end{aligned} \tag{1}$$

where $\boldsymbol{\theta}(t) = [\theta_1(t), \theta_2(t)]^{\top}$, $\dot{\boldsymbol{\theta}}(t) = d\boldsymbol{\theta}(t)/dt$,

$$\begin{aligned} D\left(\theta_2\right) &= \begin{bmatrix} \alpha_1 & \alpha_2 \cos\theta_2(t) \\ \alpha_2 \cos\theta_2(t) & \alpha_3 \end{bmatrix}, \\ \alpha_1 &= \left(m_1 + m_2\right) L_1^2 + J_1, \\ \alpha_2 &= m_2 L_1 L_2, \\ \alpha_3 &= m_2 L_2^2 + J_2, \\ \alpha_4 &= m_2 L_2 g. \end{aligned} \tag{2}$$

The Euler-Lagrange motion equations of the system are

$$\begin{aligned} \frac{d}{dt}\left[\frac{\partial L\left(\boldsymbol{\theta}, \dot{\boldsymbol{\theta}}\right)}{\partial \dot{\theta}_1}\right] - \frac{\partial L\left(\boldsymbol{\theta}, \dot{\boldsymbol{\theta}}\right)}{\partial \theta_1} &= F(t), \\ \frac{d}{dt}\left[\frac{\partial L\left(\boldsymbol{\theta}, \dot{\boldsymbol{\theta}}\right)}{\partial \dot{\theta}_2}\right] - \frac{\partial L\left(\boldsymbol{\theta}, \dot{\boldsymbol{\theta}}\right)}{\partial \theta_2} &= 0, \end{aligned} \tag{3}$$

where $L(\boldsymbol{\theta}, \dot{\boldsymbol{\theta}}) = K(\boldsymbol{\theta}, \dot{\boldsymbol{\theta}}) - P(\boldsymbol{\theta})$ is the Lagrangian of the system. Equation (3) is equivalent to

$$D\left(\theta_2\right)\begin{bmatrix} \ddot{\theta}_1(t) \\ \ddot{\theta}_2(t) \end{bmatrix} + \begin{bmatrix} -\alpha_2 \dot{\theta}_2^2(t) \sin\theta_2(t) \\ -\alpha_4 \sin\theta_2(t) \end{bmatrix} = \begin{bmatrix} F(t) \\ 0 \end{bmatrix}. \tag{4}$$

The state variables of (4) are selected to be

$$\begin{aligned} x_1(t) &= \theta_1(t), \\ x_2(t) &= \theta_2(t), \\ x_3(t) &= \dot{\theta}_1(t), \\ x_4(t) &= \dot{\theta}_2(t). \end{aligned} \tag{5}$$

This gives the state-space form of (4) as

$$\begin{aligned} \dot{x}_1(t) &= x_3(t), \\ \dot{x}_2(t) &= x_4(t), \\ \begin{bmatrix} \dot{x}_3(t) \\ \dot{x}_4(t) \end{bmatrix} &= D^{-1}\left(x_2\right)\begin{bmatrix} \alpha_2 x_4^2(t) \sin x_2(t) + F(t) \\ \alpha_4 \sin x_2(t) \end{bmatrix}. \end{aligned} \tag{6}$$

3. Dynamic Properties of the UWIP System

The UWIP system (6) has the following dynamic properties.

Theorem 1. *If the control law for (6) is designed to be*

$$F(t) = -\mu x_3(t), \quad \mu > 0, \tag{7}$$

then the closed-loop control system has two equilibrium points

$$\begin{aligned} \boldsymbol{x}_U^* &= \left[x_1^*, 0, 0, 0\right]^{\top}, \\ \boldsymbol{x}_D^* &= \left[x_1^*, \pi, 0, 0\right]^{\top}, \end{aligned} \tag{8}$$

where μ and x_1^* are constants. Moreover, $\boldsymbol{x}_D^*$ is a stable equilibrium point while $\boldsymbol{x}_U^*$ is not.

Proof. Substituting (7) into (6) yields the closed-loop control system

$$\begin{bmatrix} \dot{x}_1(t) \\ \dot{x}_2(t) \\ \dot{x}_3(t) \\ \dot{x}_4(t) \end{bmatrix} = \begin{bmatrix} x_3(t) \\ x_4(t) \\ D^{-1}(x_2)\begin{bmatrix} \alpha_2 x_4^2(t)\sin x_2(t) - \mu x_3(t) \\ \alpha_4 \sin x_2(t) \end{bmatrix} \end{bmatrix} \quad (9)$$

The equilibrium points of the system (9) satisfy

$$\begin{aligned} x_3(t) &= 0, \\ x_4(t) &= 0, \\ \begin{bmatrix} \alpha_2 x_4^2(t)\sin x_2(t) - \mu x_3(t) \\ \alpha_4 \sin x_2(t) \end{bmatrix} &= \begin{bmatrix} 0 \\ 0 \end{bmatrix}. \end{aligned} \quad (10)$$

It follows from (5) and (10) that $x_3(t) = x_4(t) = 0$, $x_1(t) = x_1^*$, and $\sin x_2(t) = 0$. By considering the fact that $x_2(t) = \theta_2(t)$ is a cyclic variable with a period 2π, it is easy to get $x_2(t) = 0$ or π from $\sin x_2(t) = 0$. So, the equilibrium points of the closed-loop control system are $\boldsymbol{x}_U^*$ and $\boldsymbol{x}_D^*$.

In order to determine the stability of the equilibrium points $\boldsymbol{x}_U^*$ and $\boldsymbol{x}_D^*$, we approximately linearize the nonlinear system (9) around them. It gives the following two approximate linearization matrices:

$$\begin{aligned} A_U^* &= \begin{bmatrix} 0 & 0 & 1 & 0 \\ 0 & 0 & 0 & 1 \\ 0 & -\dfrac{\alpha_2\alpha_4}{\alpha_1\alpha_3 - \alpha_2^2} & -\dfrac{\mu\alpha_3}{\alpha_1\alpha_3 - \alpha_2^2} & 0 \\ 0 & \dfrac{\alpha_1\alpha_4}{\alpha_1\alpha_3 - \alpha_2^2} & \dfrac{\mu\alpha_2}{\alpha_1\alpha_3 - \alpha_2^2} & 0 \end{bmatrix}, \\ A_D^* &= \begin{bmatrix} 0 & 0 & 1 & 0 \\ 0 & 0 & 0 & 1 \\ 0 & -\dfrac{\alpha_2\alpha_4}{\alpha_1\alpha_3 - \alpha_2^2} & -\dfrac{\mu\alpha_3}{\alpha_1\alpha_3 - \alpha_2^2} & 0 \\ 0 & -\dfrac{\alpha_1\alpha_4}{\alpha_1\alpha_3 - \alpha_2^2} & -\dfrac{\mu\alpha_2}{\alpha_1\alpha_3 - \alpha_2^2} & 0 \end{bmatrix}. \end{aligned} \quad (11)$$

Both A_U^* and A_D^* have the same form

$$A^* = \begin{bmatrix} 0 & 0 & 1 & 0 \\ 0 & 0 & 0 & 1 \\ 0 & A_{32} & A_{33} & 0 \\ 0 & A_{42} & A_{43} & 0 \end{bmatrix}, \quad (12)$$

where A_{ij} $(i = 3, 4,\ \ j = 2, 3)$ are constants. The characteristic polynomial of the matrix A^* is

$$\begin{aligned} &\left|sI_4 - A^*\right| \\ &\quad = s\left[s^3 - A_{33}s^2 - A_{42}s + A_{42}A_{33} - A_{32}A_{43}\right], \end{aligned} \quad (13)$$

where s is a variable symbol and I_4 is a 4×4 identity matrix. By using Routh-Hurwitz stability criterion [26], it is not difficult to obtain the stability conditions for A^* as

$$\begin{aligned} A_{33} &< 0, \\ A_{32}A_{43} &> 0, \\ A_{42}A_{33} - A_{32}A_{43} &> 0. \end{aligned} \quad (14)$$

Since $\alpha_i > 0$ $(i = 1, 2, 3, 4)$ and $\alpha_1\alpha_3 - \alpha_2^2 > 0$, a simple verification gives that A_D^* satisfies (14) and A_U^* does not. So, the equilibrium point $\boldsymbol{x}_D^*$ is stable and $\boldsymbol{x}_U^*$ is unstable. The proof is completed. □

Theorem 2. *The closed-loop control system (6) and (7) asymptotically converges to the equilibrium point $\boldsymbol{x}_D^*$ if the initial condition $\boldsymbol{x}_0^*$ is different from $\boldsymbol{x}_U^*$.*

Proof. For the closed-loop control system (6) and (7), a Lyapunov function is designed to be

$$\begin{aligned} V(\boldsymbol{x}) = {} & \frac{1}{2}[x_3, x_4]\begin{bmatrix} \alpha_1 & \alpha_2\cos x_2 \\ \alpha_2\cos x_2 & \alpha_3 \end{bmatrix}\begin{bmatrix} x_3 \\ x_4 \end{bmatrix} \\ & + \alpha_4(1 + \cos x_2). \end{aligned} \quad (15)$$

Then, we get

$$\begin{aligned} &\frac{dV(\boldsymbol{x})}{dt} \\ &= [x_3, x_4]\begin{bmatrix} \alpha_1 & \alpha_2\cos x_2 \\ \alpha_2\cos x_2 & \alpha_3 \end{bmatrix}\begin{bmatrix} \dot{x}_3 \\ \dot{x}_4 \end{bmatrix} \\ &\quad + \frac{1}{2}[x_3, x_4]\begin{bmatrix} 0 & -\alpha_2 x_4\sin x_2 \\ -\alpha_2 x_4\sin x_2 & 0 \end{bmatrix}\begin{bmatrix} x_3 \\ x_4 \end{bmatrix} \\ &\quad - \alpha_4 x_4\sin x_2 \\ &= [x_3, x_4]\begin{bmatrix} \alpha_2 x_4^2\sin x_2 - \mu x_3 \\ \alpha_4\sin x_2 \end{bmatrix} \\ &\quad - (\alpha_2 x_3 x_4 + \alpha_4) x_4\sin x_2 = -\mu x_3^2(t) \le 0. \end{aligned} \quad (16)$$

Letting $\dot{V}(\boldsymbol{x}) = 0$ gives $x_3(t) = 0$. Combining $x_3(t) = 0$ and the third equation of (4) yields

$$\left(\alpha_3 x_4^2(t) - \alpha_4\cos x_2(t)\right)\sin x_2(t) = 0. \quad (17)$$

In addition, $\dot{V}(\boldsymbol{x}) = 0$ means that $V(\boldsymbol{x}) = C$ is a constant. It follows from $x_3(t) = 0$ and $V(\boldsymbol{x}) = C$ that

$$\alpha_3 x_4^2(t) + \alpha_4\cos x_2(t) = C - \alpha_4. \quad (18)$$

Note that (17) means

$$\alpha_3 x_4^2(t) - \alpha_4\cos x_2(t) = 0 \quad (19)$$

or

$$\sin x_2(t) = 0. \quad (20)$$

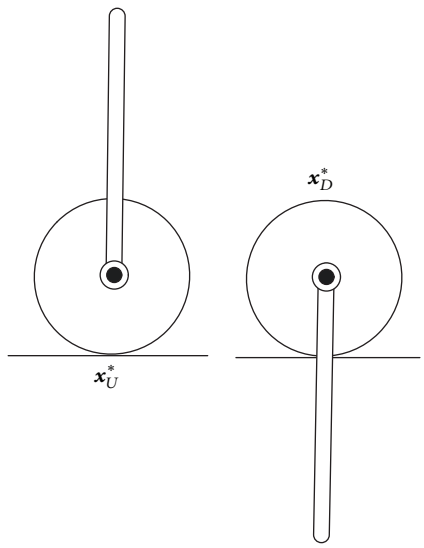

Figure 2: Physical models of x_U^* and x_D^*.

Combining (18) and (19) yields that $x_2(t)$ is a constant. The second equation of (6) gives $x_4(t) = 0$. From (19), we get $\cos x_2(t) = 0$. Furthermore, it follows from $x_3(t) = x_4(t) = 0$ and (6) that $\sin x_2(t) = 0$. It is in conflict with $\cos x_2(t) = 0$. So, (19) does not hold.

The above analysis results tell us that $x_3(t) = x_4(t) = 0$ and $\sin x_2(t) = 0$ from $\dot{V}(\boldsymbol{x}) = 0$. By using LaSalle's theorem [15], we know that the closed-loop control system (6) and (7) asymptotically converges to the largest invariant set in

$$\begin{aligned}\Omega &= \left\{\boldsymbol{x}(t) \mid x_3(t) = x_4(t) = 0,\ \sin x_2(t) = 0\right\} \\ &= \left\{\boldsymbol{x}_D^*, \boldsymbol{x}_U^*\right\}.\end{aligned} \tag{21}$$

Since $\boldsymbol{x}_U^*$ is an unstable equilibrium point of the closed-loop system (6) and (7), the system asymptotically converges to $\boldsymbol{x}_D^*$ when $\boldsymbol{x}_0^* \neq \boldsymbol{x}_U^*$. The proof is completed. □

Remark 3. The point $\boldsymbol{x}_U^*$ means that the pendulum of the UWIP is stabilized at the straight-up position while the wheel does not spin. Similarly, the meaning of $\boldsymbol{x}_D^*$ is that the pendulum is stabilized at the straight-down position while the wheel does not spin. The physical models of $\boldsymbol{x}_U^*$ and $\boldsymbol{x}_D^*$ are shown in Figure 2. Note that $x_3(t) = \dot{\theta}_1(t)$ is the velocity variable of the wheel. So, the control law $F(t)$ designed in (7) can be considered as a virtual friction torque for the UWIP system. Under the operation of this torque, the UWIP asymptotically converges to $\boldsymbol{x}_D^*$ from any initial position $\boldsymbol{x}_0^* \neq \boldsymbol{x}_U^*$. This property will be used to design a trajectory for the UWIP in its whole motion space below.

4. Design of Motion Trajectory

In this section, a motion trajectory of the UWIP between the equilibrium points $\boldsymbol{x}_D^*$ and $\boldsymbol{x}_U^*$ is designed. The design process of the trajectory has the following three steps.

Step 1. The initial condition of the closed-loop system (6) and (7) is selected to be

$$\boldsymbol{x}_0^* = \left[x_1^*, 0, \omega, 0\right]^\top, \tag{22}$$

where $\omega > 0$ is a very small constant. The physical meaning for (22) is that the UWIP starts to move from the position $\boldsymbol{x}_U^*$ with a small velocity in the wheel. Since $\boldsymbol{x}_0^* \neq \boldsymbol{x}_U^*$, it follows from the Theorem 2 that the UWIP asymptotically converges to the equilibrium point $\boldsymbol{x}_D^*$. This motion trajectory and its accompanied control input are denoted to be

$$\begin{aligned}\boldsymbol{x}_D(t) &= \left[x_{D1}(t), x_{D2}(t), x_{D3}(t), x_{D4}(t)\right]^\top, \\ F_D(t) &= -\mu x_{D3}(t), \quad t \in [0, T],\end{aligned} \tag{23}$$

where T is the stabilization time that is defined to be

$$\left\|\boldsymbol{x}_D(t) - \boldsymbol{x}_D^*\right\|_2 \leq 0.05, \quad t \geq T. \tag{24}$$

Equation (24) means that $\boldsymbol{x}_D(t) = \boldsymbol{x}_D^*$ approximately holds when $t \geq T$.

Step 2. Based on $\boldsymbol{x}_D(t)$ and $F_D(t)$, we construct

$$\begin{aligned}\boldsymbol{x}_U(t) &= \left[x_{U1}(t), x_{U2}(t), x_{U3}(t), x_{U4}(t)\right]^\top, \\ x_{U1}(t) &= x_{D1}(T - t), \\ x_{U2}(t) &= x_{D2}(T - t), \\ x_{U3}(t) &= -x_{D3}(T - t), \\ x_{U4}(t) &= -x_{D4}(T - t), \\ F_U(t) &= F_D(T - t), \quad t \in [0, T].\end{aligned} \tag{25}$$

Note that $x_{D1}(t)$ and $x_{D2}(t)$ are the position variables, and $x_{D3}(t)$ and $x_{D4}(t)$ are the velocity variables of the UWIP system. Thus, $\boldsymbol{x}_U(t)$ is a reverse trajectory of $\boldsymbol{x}_D(t)$ during $t \in [0, T]$. And the initial and final positions of $\boldsymbol{x}_U(t)$ are

$$\begin{aligned}\boldsymbol{x}_U(0) &= \left[x_{D1}(T), x_{D2}(T), -x_{D3}(T), -x_{D4}(T)\right]^\top \\ &\approx \boldsymbol{x}_D^*, \\ \boldsymbol{x}_U(T) &= \left[x_{D1}(0), x_{D2}(0), -x_{D3}(0), -x_{D4}(0)\right]^\top \\ &= \left[x_1^*, 0, -\omega, 0\right]^\top \triangleq \widetilde{\boldsymbol{x}}_0^*.\end{aligned} \tag{26}$$

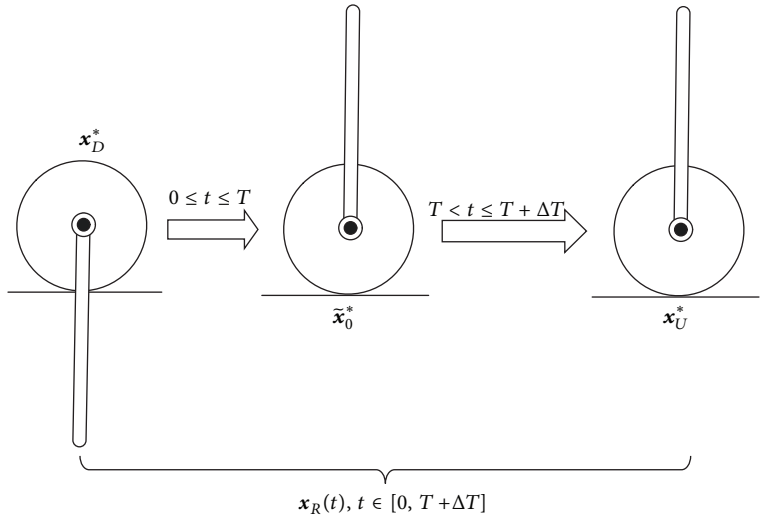

Figure 3: The diagram of the trajectory $x_R(t)$.

Let $v = T - t$. Since $x_D(t)$ and $F_D(t)$ satisfy (6), we get

$$\begin{aligned}
\frac{dx_{U1}(t)}{dt} &= \frac{dx_{U1}(t)}{dv}\frac{dv}{dt} = -\frac{dx_{D1}(v)}{dv} = -x_{D3}(v) \\
&= x_{U3}(t), \\
\frac{dx_{U2}(t)}{dt} &= \frac{dx_{U2}(t)}{dv}\frac{dv}{dt} = -\frac{dx_{D2}(v)}{dv} = -x_{D4}(v) \\
&= x_{U4}(t), \\
\begin{bmatrix} \frac{dx_{U3}(t)}{dt} \\ \frac{dx_{U4}(t)}{dt} \end{bmatrix} &= \begin{bmatrix} \frac{dx_{U3}(t)}{dv}\frac{dv}{dt} \\ \frac{dx_{U4}(t)}{dv}\frac{dv}{dt} \end{bmatrix} = \begin{bmatrix} \frac{dx_{D3}(v)}{dv} \\ \frac{dx_{D4}(v)}{dv} \end{bmatrix} \\
&= D^{-1}\left(x_{D2}(v)\right)\begin{bmatrix} \alpha_2 x_{D4}^2(v)\sin x_{D2}(v) + F_D(v) \\ \alpha_4 \sin x_{D2}(v) \end{bmatrix} \\
&= D^{-1}\left(x_{U2}(t)\right)\begin{bmatrix} \alpha_2 x_{U4}^2(t)\sin x_{U2}(t) + F_U(t) \\ \alpha_4 \sin x_{U2}(t) \end{bmatrix}.
\end{aligned} \tag{27}$$

This means that $x_U(t)$ and $F_U(t)$ satisfy (6).

Step 3. Since the constant ω is very small, $\tilde{x}_0^*$ is very close to the equilibrium point x_U^*. It enables us to introduce a time period ΔT and to define

$$\begin{aligned}
x_R(t) &= \left[x_{R1}(t), x_{R2}(t), x_{R3}(t), x_{R4}(t)\right]^\top, \\
x_R(t) &= \begin{cases} x_U(t), & t \in [0, T], \\ x_U^*, & t \in (T, T + \Delta T], \end{cases} \\
F_R(t) &= \begin{cases} F_U(t), & t \in [0, T], \\ 0, & t \in (T, T + \Delta T]. \end{cases}
\end{aligned} \tag{28}$$

The diagram of the trajectory $x_R(t)$ is shown in Figure 3. Note that $x_R(t)$ is a motion trajectory of the UWIP between the equilibrium points x_D^* and x_U^*. By comparing $x_U(T)$ to x_U^*, we find that the element $x_{R3}(t)$ in $x_R(t)$ suffers from a very small step change at $t = T$. Furthermore, it is not difficult to verify that $x_R(t)$ and $F_R(t)$ also satisfy (6) because $x_U(t)$ and $F_U(t)$ satisfy (6).

5. Design of Tracking Control Law

The design of tracking control law for the trajectory $x_R(t)$ is concerned in this section. Denote the error variables to be

$$\begin{aligned}
e(t) &= \left[e_1(t), e_2(t), e_3(t), e_4(t)\right]^\top, \\
e_1(t) &= x_1(t) - x_{R1}(t), \\
e_2(t) &= x_2(t) - x_{R2}(t), \\
e_3(t) &= x_3(t) - x_{R3}(t), \\
e_4(t) &= x_4(t) - x_{R4}(t), \\
\tau(t) &= F(t) - F_R(t).
\end{aligned} \tag{29}$$

From (6), we get the nonlinear error dynamic equations as

$$\begin{bmatrix} \dot{e}_1(t) \\ \dot{e}_2(t) \\ \dot{e}_3(t) \\ \dot{e}_4(t) \end{bmatrix} = \begin{bmatrix} e_3(t) \\ e_4(t) \\ f_1(e) \\ f_2(e) \end{bmatrix} + \begin{bmatrix} 0 \\ 0 \\ g_1(e) \\ g_2(e) \end{bmatrix}\tau(t), \tag{30}$$

where

$$\begin{bmatrix} f_1(\boldsymbol{e}) \\ f_2(\boldsymbol{e}) \end{bmatrix} = \Phi^{-1}(e_2)\left(\phi_1(e_2) + \phi_2(\boldsymbol{e})\right),$$

$$\begin{bmatrix} g_1(\boldsymbol{e}) \\ g_2(\boldsymbol{e}) \end{bmatrix} = \Phi^{-1}(e_2)\begin{bmatrix} 1 \\ 0 \end{bmatrix},$$

$$\phi_1(e_2) = \begin{bmatrix} -\alpha_2 \dot{x}_{R4}\left(\cos(e_2 + x_{R2}) - \cos x_{R2}\right) \\ -\alpha_2 \dot{x}_{R3}\left(\cos(e_2 + x_{R2}) - \cos x_{R2}\right) \end{bmatrix}, \tag{31}$$

$$\phi_2(\boldsymbol{e}) = \begin{bmatrix} \alpha_2\left((e_4 + x_{R4})^2 \sin(e_2 + x_{R2}) - x_{R4}^2 \sin x_{R2}\right) \\ \alpha_4\left(\sin(e_2 + x_{R2}) - \sin x_{R2}\right) \end{bmatrix},$$

$$\Phi(e_2) = \begin{bmatrix} \alpha_1 & \alpha_2 \cos(e_2 + x_{R2}) \\ \alpha_2 \cos(e_2 + x_{R2}) & \alpha_3 \end{bmatrix}.$$

In order to make the UWIP track the trajectory $\boldsymbol{x}_R(t)$, we need to design a stabilizing control law $\tau(t)$ for (30) such that $\boldsymbol{e}(t)$ converges to the origin quickly.

Note that (30) is a complex nonlinear control system for $\boldsymbol{e}(t)$. An approximate linearization method is used to design the stabilizing control law here. Linearizing (30) around $\boldsymbol{e}(t) = 0$ gives the following linear approximation model:

$$\dot{\boldsymbol{e}}(t) = A(t)\,\boldsymbol{e}(t) + B(t)\,\tau(t), \tag{32}$$

where

$$A(t) = \begin{bmatrix} 0 & 0 & 1 & 0 \\ 0 & 0 & 0 & 1 \\ 0 & \Psi_1(t) & \Psi_2(t) & 0 \\ 0 & \Psi_3(t) & \Psi_4(t) & 0 \end{bmatrix},$$

$$B(t) = \begin{bmatrix} 0 \\ 0 \\ \Psi_5(t) \\ \Psi_6(t) \end{bmatrix},$$

$$\Psi_1(t) = \frac{\alpha_2\alpha_3\varphi_1(t) - \alpha_2 \cos x_{R2}(t)\,\varphi_2(t)}{\alpha_1\alpha_3 - \alpha_2^2 \cos^2 x_{R2}(t)},$$

$$\Psi_2(t) = \frac{2\alpha_2\alpha_3 x_{R4}(t) \sin x_{R2}(t)}{\alpha_1\alpha_3 - \alpha_2^2 \cos^2 x_{R2}(t)},$$

$$\Psi_3(t) = \frac{-\alpha_2^2 \cos x_{R2}(t)\,\varphi_1(t) + \alpha_1\varphi_2(t)}{\alpha_1\alpha_3 - \alpha_2^2 \cos^2 x_{R2}(t)},$$

$$\Psi_4(t) = -\frac{2\alpha_2^2 x_{R4}(t) \sin x_{R2}(t) \cos x_{R2}(t)}{\alpha_1\alpha_3 - \alpha_2^2 \cos^2 x_{R2}(t)},$$

$$\Psi_5(t) = \frac{\alpha_3}{\alpha_1\alpha_3 - \alpha_2^2 \cos^2 x_{R2}(t)},$$

$$\Psi_6(t) = -\frac{\alpha_2 \cos x_{R2}(t)}{\alpha_1\alpha_3 - \alpha_2^2 \cos^2 x_{R2}(t)},$$

$$\varphi_1(t) = \dot{x}_{R4}(t) \sin x_{R2}(t) + x_{R4}^2(t) \cos x_{R2}(t),$$

$$\varphi_2(t) = \alpha_2 \dot{x}_{R3}(t) \sin x_{R2}(t) + \alpha_4 \cos x_{R2}(t). \tag{33}$$

Assume that $(A(t), B(t))$ is controllable. So, the time-variant Ricatti matrix equation

$$\dot{P}(t) + A^{\top}(t)\,P(t) + P(t)\,A(t) - P(t)\,B(t)\,R^{-1}B^{\top}(t)\,P(t) + Q = 0 \tag{34}$$

has a positive definite solution $P(t)$, where $Q \in \mathbb{R}^{4\times4}$ is a positive definite matrix and R is a positive constant. Based on the quadratic optimal control theory, the control law

$$\tau(t) = -R^{-1}B^{\top}(t)\,P(t) \tag{35}$$

stabilizes the error dynamic equation (32) at the origin quickly. As a result, the control law $F(t) = \tau(t) + F_R(t)$ enables the UWIP quickly to track the trajectory $\boldsymbol{x}_R(t)$. This guarantees the control objective of swing the UWIP up from $\boldsymbol{x}_D^*$ and stabilizing it at $\boldsymbol{x}_U^*$ to be achieved.

6. Numerical Example

This section presents a numerical example to verify the validity of the above theoretical analysis results.

The physical parameters of the UWIP in [25] were chosen for simulations

$$\begin{aligned} m_1 &= 1\,\text{kg}, \\ m_2 &= 2\,\text{kg}, \\ L_1 &= 0.1\,\text{m}, \\ L_2 &= 0.2\,\text{m}, \\ J_1 &= 0.01\,\text{kg}\cdot\text{m}^2, \\ J_2 &= 0.0267\,\text{kg}\cdot\text{m}^2. \end{aligned} \tag{36}$$

And the parameters in (7) and (22) were selected to be

$$\begin{aligned} \mu &= 0.25, \\ x_1^* &= 0, \\ \omega &= 0.001. \end{aligned} \tag{37}$$

The sampling period for simulations was chosen to be 0.001 s. From the design process in Step 1 of Section 4, we got the trajectory $\boldsymbol{x}_D(t)$ (see Figure 4). The simulation result shows that the UWIP starts to move from the position $\boldsymbol{x}_0^*$ in (22) and is stabilized at the position $\boldsymbol{x}_D^*$ in (8). The stabilizing

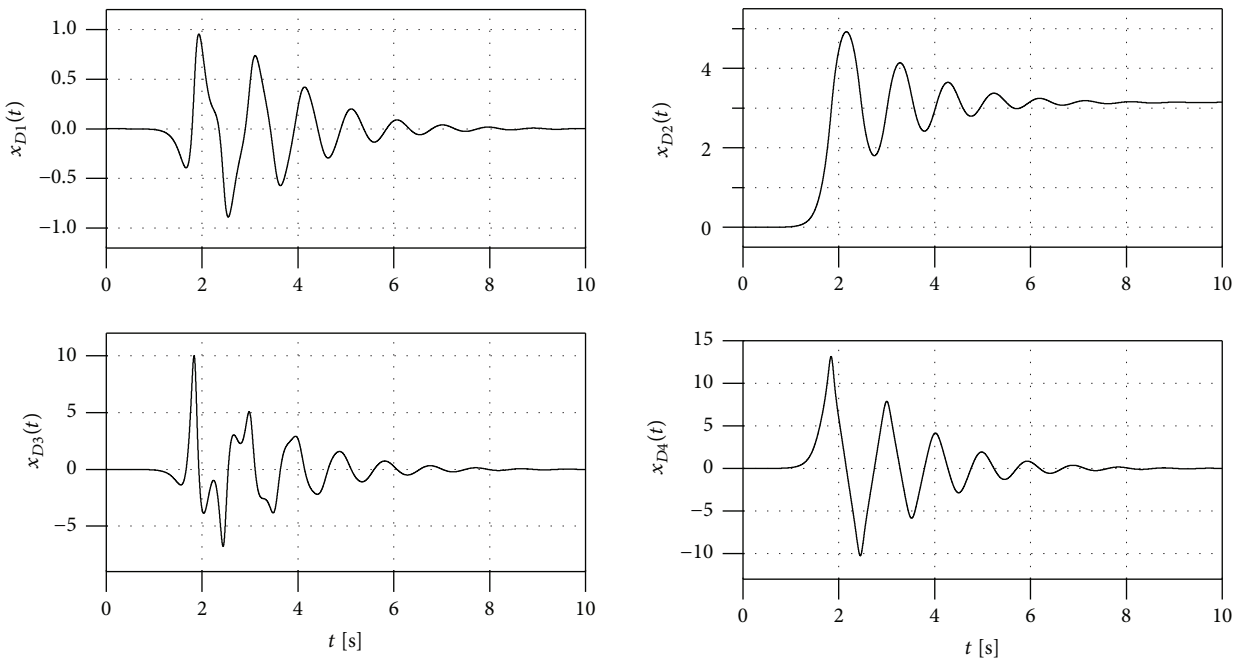

FIGURE 4: Simulation result of the trajectory $\boldsymbol{x}_D(t)$.

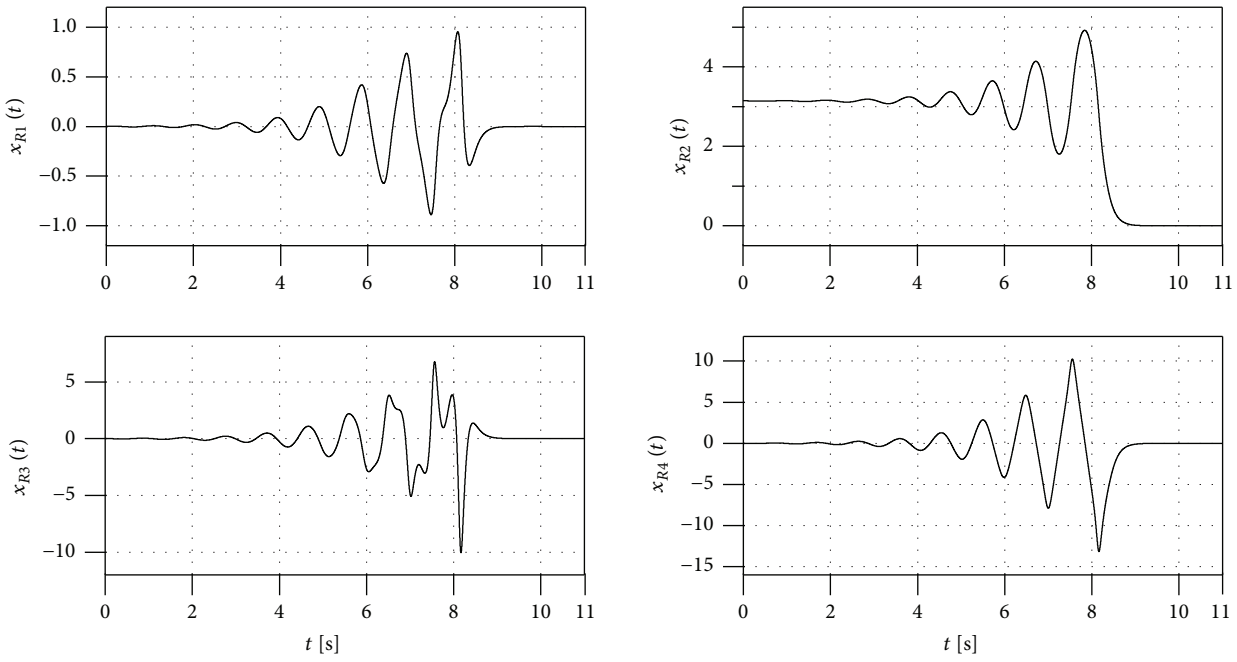

FIGURE 5: Time response of the trajectory $\boldsymbol{x}_R(t)$.

motion process of the UWIP is smooth. And the stabilization time is $T = 10$ s. This demonstrates the effectiveness of the Theorem 2.

The time period ΔT in (28) was taken to be 1 s. From the design process in Steps 2 and 3 of Section 4, the trajectory $\boldsymbol{x}_R(t)$ was obtained in Figure 5 based on $\boldsymbol{x}_D(t)$, (25), and (28). The simulation results in Figure 5 show that $\boldsymbol{x}_R(t)$ is a motion trajectory of the UWIP from $\boldsymbol{x}_D^*$ to $\boldsymbol{x}_U^*$. To design a control law of tracking this trajectory, the parameters in (34) were chosen to be $Q = 0.5I_4$ and $R = 5$. And the MATLAB function *LQR* was used to solve (34). The tracking control results for the desired trajectory $\boldsymbol{x}_R(t)$ are shown in Figure 6. Note that the UWIP quickly and exactly tracks the $\boldsymbol{x}_R(t)$ by the operation of our designed tracking control law. As a result, the stabilizing control of the UWIP from $\boldsymbol{x}_D^*$ to $\boldsymbol{x}_U^*$ is achieved along the trajectory $\boldsymbol{x}_R(t)$.

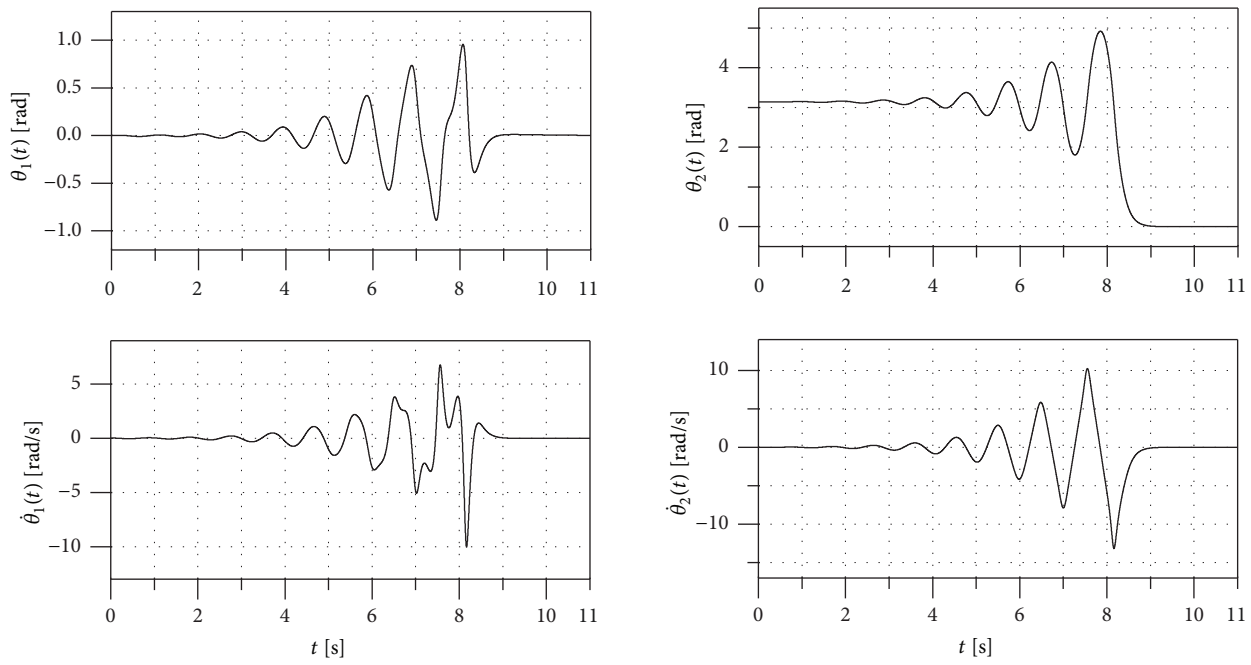

Figure 6: Tracking control of the UWIP for the trajectory $\boldsymbol{x}_R(t)$.

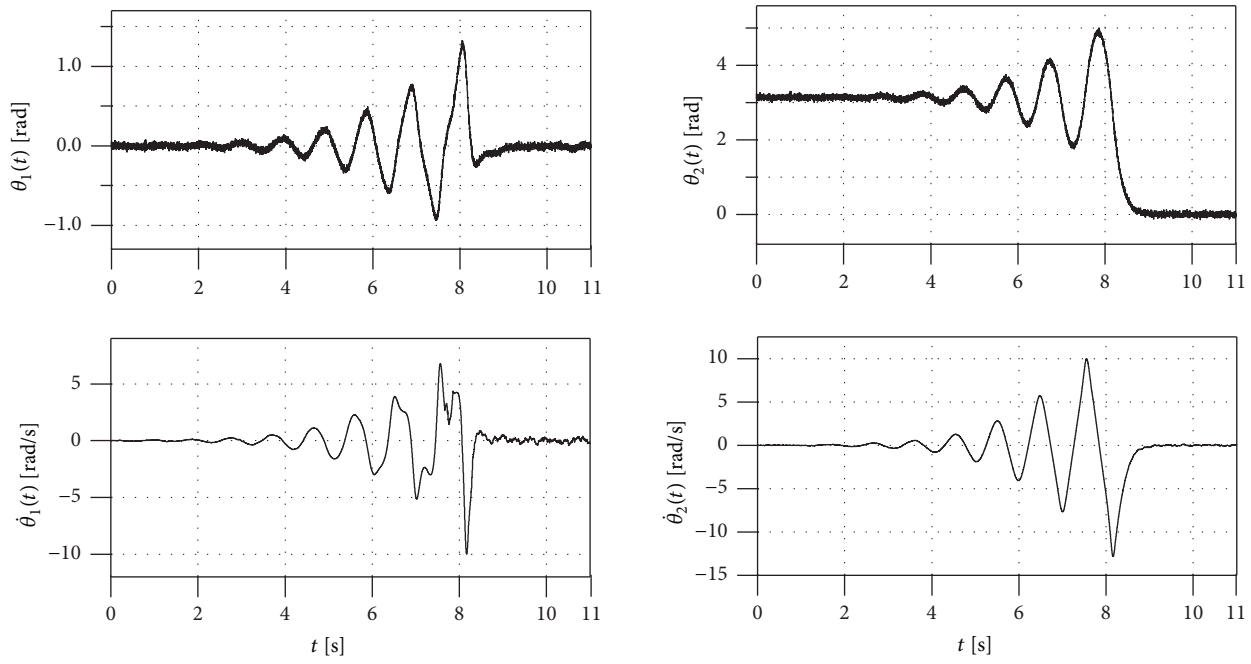

Figure 7: Simulation results of tracking $\boldsymbol{x}_R(t)$ when considering parameter uncertainties, external disturbances, and input saturation.

In order to show the applicability of the presented strategy under realistic conditions, its robustness needs to be verified. To do that, we took the parameter J_1 to be 5% smaller and J_2 to be 5% larger than their nominal values, added white noise disturbances to the measured variable (peak value: ±0.1), and set the saturation range of input to be [-3.5, 3]. Simulation results show that our developed method is still effective in that case (see Figure 7).

7. Conclusion

This paper addressed the trajectory design and tracking control problems for an underactuated wheeled inverted pendulum (UWIP). A new motion planning strategy was developed for this underactuated system. First, the dynamic properties of the UWIP system were analyzed. And then, the analysis properties were used to construct a trajectory of the

UWIP between two equilibrium points. After that, a control law was designed to make the UWIP track the constructed trajectory. This ensured the motion control of the UWIP between two equilibrium points to be achieved. Finally, numerical simulation results demonstrated the validity of our theoretical results. In the future, we will further explore how to extend the main idea of our presented method to the control of other nonlinear systems.

Data Availability

The simulation data used to support the findings of this study are available from the corresponding author upon request.

Conflicts of Interest

The authors declare that there are no conflicts of interest regarding the publication of this article.

Acknowledgments

This work was supported in part by National Natural Science Foundation of China under Grants nos. 61773193, 61703194, and 61873348, by the program of JSPS (Japan Society for the Promotion of Science) International Research Fellows under Grant no. 17F17791, and by the project of Young Teacher Growth Program of Shandong Province.

References

[1] X. Hao, L. Liu, and Y. Wu, "Existence and multiplicity results for nonlinear periodic boundary value problems," *Nonlinear Analysis: Theory, Methods & Applications*, vol. 72, no. 9-10, pp. 3635–3642, 2010.

[2] Y. Han, X. Zhang, L. Liu, and Y. Wu, "Multiple Positive Solutions of Singular Nonlinear Sturm-Liouville Problems with Carathéodory Perturbed Term," *Journal of Applied Mathematics*, vol. 2012, Article ID 160891, 23 pages, 2012.

[3] X. Hao, L. Liu, and Y. Wu, "Positive solutions for nonlinear fractional semipositone differential equation with nonlocal boundary conditions," *Journal of Nonlinear Sciences and Applications. JNSA*, vol. 9, no. 6, pp. 3992–4002, 2016.

[4] B. Zhu, L. Liu, and Y. Wu, "Local and global existence of mild solutions for a class of nonlinear fractional reaction-diffusion equations with delay," *Applied Mathematics Letters*, vol. 61, pp. 73–79, 2016.

[5] W. Qi, J. H. Park, J. Cheng, Y. Kao, and X. Gao, "Anti-windup design for stochastic Markovian switching systems with mode-dependent time-varying delays and saturation nonlinearity," *Nonlinear Analysis: Hybrid Systems*, vol. 26, pp. 201–211, 2017.

[6] L. Liu, H. Li, C. Liu, and Y. Wu, "Existence and uniqueness of positive solutions for singular fractional differential systems with coupled integral boundary conditions," *The Journal of Nonlinear Science and its Applications*, vol. 10, no. 1, pp. 243–262, 2017.

[7] Y. Sun, L. Liu, and Y. Wu, "The existence and uniqueness of positive monotone solutions for a class of nonlinear Schrödinger equations on infinite domains," *Journal of Computational and Applied Mathematics*, vol. 321, pp. 478–486, 2017.

[8] W. Qi, G. Zong, and H. R. Karim, "Observer-Based Adaptive SMC for Nonlinear Uncertain Singular Semi-Markov Jump Systems With Applications to DC Motor," *IEEE Transactions on Circuits and Systems I: Regular Papers*, vol. 65, no. 9, pp. 2951–2960, 2018.

[9] A. Zhang, X. Lai, M. Wu, and J. She, "Stabilization of underactuated two-link gymnast robot by using trajectory tracking strategy," *Applied Mathematics and Computation*, vol. 253, pp. 193–204, 2015.

[10] W. Dong and Y. Guo, "Global time-varying stabilization of underactuated surface vessel," *IEEE Transactions on Automatic Control*, vol. 50, no. 6, pp. 859–864, 2005.

[11] X. Wang, J. Liu, and K. Cai, "Tracking control for a velocity-sensorless VTOL aircraft with delayed outputs," *Automatica*, vol. 45, no. 12, pp. 2876–2882, 2009.

[12] N. Sun and Y. Fang, "Nonlinear tracking control of underactuated cranes with load transferring and lowering: theory and experimentation," *Automatica*, vol. 50, no. 9, pp. 2350–2357, 2014.

[13] D. A. Mercado Ravell, M. M. Maia, and F. J. Diez, "Modeling and control of unmanned aerial/underwater vehicles using hybrid control," *Control Engineering Practice*, vol. 76, pp. 112–122, 2018.

[14] I. Meza, L. Aguilar, A. Shiriaev, L. Freidovich, and Y. Orlov, "Periodic motion planning and nonlinear H_∞ tracking control of a 3-DOF underactuated helicopter," *International Journal of Systems Science*, vol. 42, no. 5, pp. 829–838, 2011.

[15] H. Khalil, *Nonlinear Systems*, Prentice-Hall, New Jersey, NJ, USA, 3rd edition, 2002.

[16] G. Oriolo and Y. Nakamura, "Control of mechanical systems with second-order nonholonomic constraints: Underactuated manipulators," in *Proceedings of the 30th IEEE Conference on Decision and Control (Part 1 of 3)*, pp. 2398–2403, December 1991.

[17] X. Xin and M. Kaneda, "Analysis of the energy-based swing-up control of the Acrobot," *International Journal of Robust and Nonlinear Control*, vol. 17, no. 16, pp. 1503–1524, 2007.

[18] M. Ramírez-Neria, H. Sira-Ramírez, R. Garrido-Moctezuma, and A. Luviano-Juárez, "Linear active disturbance rejection control of underactuated systems: the case of the Furuta pendulum," *ISA Transactions®*, vol. 53, no. 4, pp. 920–928, 2014.

[19] M. K. Choudhary and G. Naresh Kumar, "ESO based LQR controller for ball and beam system," *IFAC-PapersOnLine*, vol. 49, no. 1, pp. 607–610, 2016.

[20] F. Celani, "Output regulation for the TORA benchmark via rotational position feedback," *Automatica*, vol. 47, no. 3, pp. 584–590, 2011.

[21] J. She, A. Zhang, X. Lai, and M. Wu, "Global stabilization of 2-DOF underactuated mechanical systems—an equiavlent-input-disturbance approach," *Nonlinear Dynamics*, vol. 69, no. 1-2, pp. 495–509, 2012.

[22] X. Lai, J. She, S. X. Yang, and M. Wu, "Comprehensive unified control strategy for underactuated two-link manipulators," *IEEE Transactions on Systems, Man, and Cybernetics, Part B: Cybernetics*, vol. 39, no. 2, pp. 389–398, 2009.

[23] X. Xin and Y. Liu, "Reduced-order stable controllers for two-link underactuated planar robots," *Automatica*, vol. 49, no. 7, pp. 2176–2183, 2013.

[24] J. G. Romero, A. Donaire, R. Ortega, and P. Borja, "Global Stabilisation of Underactuated Mechanical Systems via PID Passivity-Based Control," *IFAC-PapersOnLine*, vol. 50, no. 1, pp. 9577–9582, 2017.

[25] Y. Ge, A. Zhang, J. Huo, S. Duan, L. Wang, and J. Kang, "Modeling and stabilizing control of wheeled acrobatic robot," *Application in Automation*, vol. 2017, no. 3, pp. 101–103, 2017.

[26] J. Huang, *Automatic Control Principles and Applications*, Higher education press, Beijing, China, 2nd edition, 2009.